Simultaneous Surface-Enhanced Raman Spectroscopy (SERS) and Atomic Force Microscopy (AFM) for Label-Free Physicochemical Analysis of Lipid Bilayers

CLAIRE S. SWEETENHAM,* MARTA LARRAONA-PUY,* and IOAN NOTINGHER†

Nanoscience Group, School of Physics and Astronomy, University of Nottingham, University Park, Nottingham, NG7 2RD, UK

Large-scale two-dimensional (2D) arrays of metallic nanostructures formed by thin-film evaporation over hexagonally close-packed polystyrene spheres are established substrates for surface-enhanced Raman spectroscopy (SERS). By using these substrates with an integrated atomic force microscopy (AFM) and inverted Raman spectroscopy system, simultaneous topographical imaging and high-sensitivity chemical mapping can be performed. In this paper, we have used this technique to investigate supported bilayers of long-chain fatty acids and phospholipids deposited by the Langmuir–Blodgett (LB) and spin-coating techniques. Nanosphere lithography (NSL) substrates created from 384 and 1002 nm polystyrene spheres and silver (Ag) deposition on glass and sapphire substrates were characterized for SERS in terms of their structure, distribution, and level of enhancement. SERS mappings of rhodamine 6G (R6G) and p-aminothiophenol (p-ATP) monolayers on the 384 nm substrates demonstrate high and uniform enhancement at a micrometer scale. The enhancement was sufficiently high to enable measurement of SERS spectra for arachidic acid (AA) and dipalmitoylphosphatidylcholine (DPPC) layers on sapphire/Ag substrates. The roughness of these substrates (<2 nm) was lower than for glass/Ag (~5 nm); therefore, simultaneous to SERS it was possible to measure the topography of the samples by AFM and determine the number of layers of AA and DPPC. This study shows the potential of the combined AFM/SERS technique for spectral and topographical characterization of phospholipid bilayers. This may prove to be an interesting approach for further studies with more complex heterogeneous lipid mixtures aiming to measure spatially resolved features such as microdomains.

Index Headings: **Supported lipid bilayers; Atomic force microscopy; AFM; Surface-enhanced Raman spectroscopy; SERS; Nanosphere lithography.**

INTRODUCTION

Supported lipid bilayers (SLB) provide a biologically relevant model for cell membranes, with the ability to manipulate and modify the makeup and environment of the bilayers in order to give a fair representation of the cellular system being depicted. These nanoscale structures consist of phospholipid molecules that self-organize into phase-separated areas, which are also known as microdomains.[1,2]

A wide range of imaging techniques has been used to study SLBs. Atomic force microscopy (AFM) has been employed extensively to characterize lipid bilayers, providing high-resolution images and mechanical information at the nanoscale. This technique has revealed the formation and nanoscale organization of lipid bilayers, monitored the inclusion of biomolecules and proteins, and investigated interactions with external agents such as drugs and nanoparticles.[3] Mass spectrometry has been employed to analyze the chemical composition of lipid bilayers.[4,5] Nuclear magnetic resonance (NMR) spectroscopy,[6] X-ray diffraction, and neutron scattering[7] have been used to investigate the structure of lipid bilayers in vesicles and also their interaction with proteins. Fluorescence microscopy has been used to study the interaction of proteins and other biomolecules within a lipid bilayer[8] and the movement of charged components across them.[9] The technique has also been combined with AFM to investigate the growth, shape, and topology of microdomains.[10] However, the main limitations of these techniques is that they are destructive or require labeling of the molecules of interest, which may disturb the structure of the bilayers. In addition, there is a limited availability of fluorescent labels such as those for cholesterol, which is an important membrane lipid known to play a key role in the properties of microdomains. Also for studies of vesicles in solution, as in NMR spectroscopy, it has not been possible to correlate chemical information with spatial features, which is required to discriminate molecular interactions within the liquid ordered regions corresponding to microdomains from the rest of the liquid disordered membrane.

Conventional non-resonant Raman spectroscopy lacks the sensitivity required to image single or stacks of few lipid bilayers due to their small scale and weak Raman scattering. The addition of optical trapping has enabled the detection of lipid bilayers within single vesicles.[11] A total internal reflection (TIR) geometry has been used to enhance the Raman scattering from lipid bilayers.[12] However, these methods do not provide spatially resolved information about the bilayers. Coherent anti-Stokes Raman spectroscopy (CARS) benefits from increased sensitivity,[13] but its reduced spectral discrimination, particularly in the fingerprint spectral region (600–1800 cm^{-1}), makes it difficult to discriminate between various lipid species.[14,15]

One combination of techniques that has the potential to topographically, mechanically, and chemically investigate lipid bilayers with high spatial resolution is AFM combined with surface-enhanced Raman spectroscopy (SERS). The technique is noninvasive, label-free, and can perform real-time measurements on SLBs in aqueous environment. SERS has been used to study so-called hybrid bilayers; these bilayers contain a lipid monolayer tethered to a metal substrate,[16] electrode,[17] or nanoshell[18] by a self-assembled monolayer of alkanethiols. Also, lipid bilayers have been detected on SERS substrates in combination with techniques such as resonance Raman[19,20] and TIR.[21] However, in none of these reports were the techniques able to obtain spatially resolved information.

The aim of this paper is to investigate whether supported bilayers of fatty acids and phospholipids can be topographically and chemically investigated simultaneously by using an integrated AFM–Raman technique. Nanosphere lithography

Received 11 April 2011; accepted 7 September 2011.
* These authors contributed equally to this work.
† Author to whom correspondence should be sent. E-mail: ioan.notingher@nottingham.ac.uk.
DOI: 10.1366/11-06319

0003-7028/11/6512-1387$2.00/0

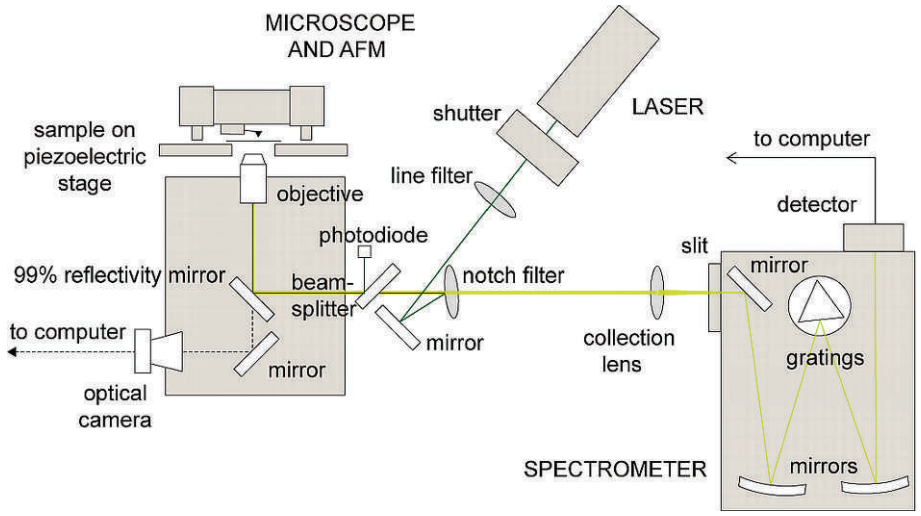

FIG. 1. Schematic of combined AFM and Raman spectroscopy system.

(NSL) SERS substrates, based on flat sapphire with roughness below 2 nm, allow accurate imaging of the bilayers by AFM. These substrates are more useful than glass/Ag substrates as potentially even height differences of the order of 1–2 nm needed for imaging microdomains could be measured. Simultaneous AFM topography and SERS measurements are then presented for long-chain fatty acids (arachidic acid) and a cationic phospholipid (ethyl-dipalmitoylphosphatidylcholine).

EXPERIMENTAL METHODS

Instrumental Setup and Data Analysis. Surface-enhanced Raman spectroscopy measurements were performed on a purpose-built Raman spectroscopy system with integrated AFM optimized for characterizing and studying lipid bilayers (Fig. 1).[22] A 20 μW 532 nm continuous wave laser (Laser 2000, UK) is directed through the inverted microscope (IX71, Olympus, Japan) and focused onto the sample by a water-immersion 1.2 NA 60× objective (UPLSAPO, Olympus), producing a laser spot approximately 0.5 μm in diameter on the sample. Raman scattered photons are collected by the same objective and analyzed by a double Czerny–Turner Raman spectrometer equipped with a 1800 lines/mm ruled grating and a back-illuminated charge-coupled device (CCD, Andor Technologies, UK). Topography images are measured with an AFM (Nanowizard, JPK Instruments, Germany) with a piezoelectric x–y-stage fitted to the Raman microscope. The AFM is used in tapping and contact mode in air with rectangular silicon probes (70 kHz resonant frequency and 2 N/m spring constant, AC240TS, Asylum Research, UK). A dichroic beam splitter and a silicon photodiode were added to improve the alignment between the Raman laser and the AFM tip. Accurate lateral alignment between the AFM tip and excitation laser is carried out using the tip-assisted optics (TAO) module by scanning the tip through the laser spot and locking it at the position of maximum scattering intensity.

Raman spectra were preprocessed in MATLAB (MathWorks, Natick, MA) following the procedure described elsewhere.[23]

SERS-Active Substrates. Large-scale, two-dimensional (2D) arrays of truncated tetrahedral nanostructures were formed[24] to create NSL SERS-active substrates.[25] A process similar to the one described previously[22] using polystyrene spheres with diameters of 384 and 1002 nm, 10 wt.% in water (Varian, Inc), was used. Large areas of highly ordered hexagonally close-packed monolayers of polystyrene spheres were deposited on glass (VWR, UK) or sapphire (PI-KEM, UK). An approximately 25 nm thin film of Ag was deposited with a thermal evaporator in vacuum (Edwards, USA), then the polystyrene spheres were removed by immersing the substrates in tetrahydrofuran (Sigma-Aldrich, UK) for 15 min and then ultrasonicated for 20 s, followed by washing with ethanol and drying in a N_2 stream.

Molecular Monolayers and Lipid Layers. All chemicals and solvents (analytical grade) were used without any further purification (Sigma-Aldrich). The SERS activity of these substrates was assessed with monolayers of rhodamine 6G (R6G), a dye molecule that attaches to both the silver regions and the substrate (glass or sapphire), and p-aminothiophenol (p-ATP), an aromatic compound that strongly bonds to silver due to its thiol group. The SERS substrates were immersed in 1 mM R6G and 10^{-4} M p-ATP methanol solutions for 2 h and then rinsed in methanol to ensure a single molecular layer was adsorbed.[22,26] Layers of arachidic acid (AA), a saturated fatty acid molecule, were formed using a Langmuir–Blodgett (LB) trough (Nima Technology, UK). Neutral 1,2-dihexadecanoyl-*sn*-glycero-3-phosphocholine (DPPC) and charged 1,2-dihexadecanoyl-*sn*-glycero-3-ethylphosphocholine (cationic-DPPC) (Avanti Polar Lipids, USA) were dissolved in organic solvents and deposited on the sapphire/Ag substrates by LB or spin coating. For the spin-coating technique, a hydrophilic solvent (2-propanol) was chosen over hydrophobic solvents (chloroform) to improve the wetting of hydrophilic substrates and to control the solvent evaporation.

RESULTS AND DISCUSSION

Characterization of SERS Substrates. The first requirement for imaging SLBs with Raman spectroscopy is to produce SERS substrates with high, consistent, and uniform enhancement of Raman scattering. The dimensions and large-scale ordering of the silver-truncated tetrahedral nanostructures makes these SERS substrates ideally suited for such applications. Collective resonances from areas of tens of micrometers

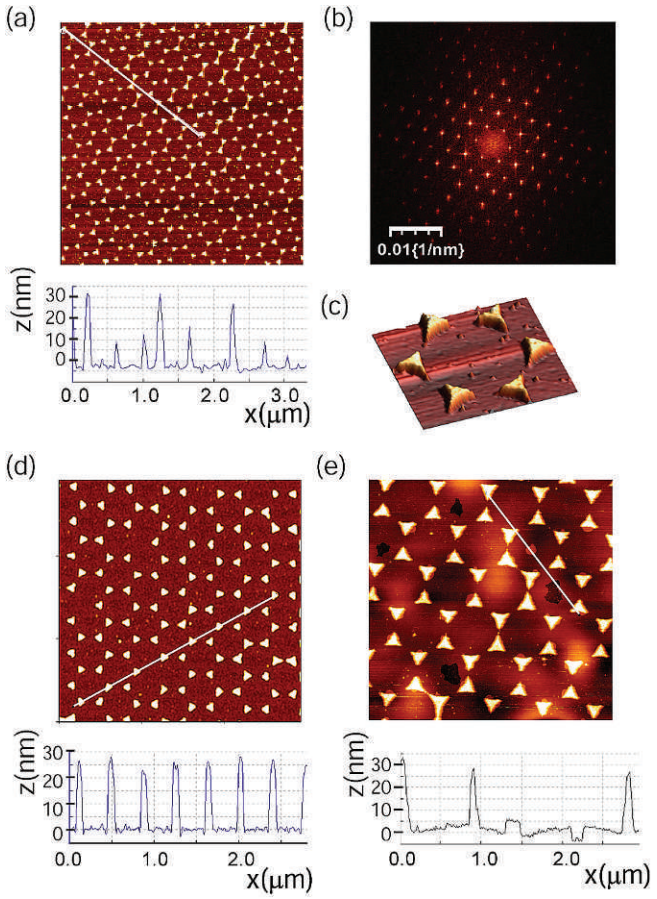

FIG. 2. AFM topographical characterization of the NSL substrates. (**a**) Glass/Ag substrate profile shows roughness of 5–10 nm while sapphire/Ag substrates (**d**) have typical roughness below 2 nm. (**e**) DPPC multilayer deposition on sapphire/Ag substrate. (**b**) and (**c**) are the 2D FFT of a larger image of (a) and a 3D representation of the truncated silver nanostructures.

of these nanostructures are key to achieving localized electric field optimization and in turn optimized SERS activity. AFM images of such SERS substrates are shown in Fig. 2, from which the size of individual nanostructures and the extent of ordering across the substrate is apparent. In addition, a 2D fast Fourier transform (FFT) was measured for large AFM images of the substrates (Fig. 2b); the concentric periodic structure indicates the length scale of the nanostructures within the substrate and, more importantly, high hexagonal order. This data demonstrates the potential of these substrates for activation of SERS; however, the level and distribution of this enhancement across the substrates can be explored by further analysis with SERS mapping.

Figure 2 also enables a comparison between typical glass/Ag and sapphire/Ag SERS substrates. Glass surface roughness is found to be 5–10 nm, while it is below 2 nm for sapphire. The lower roughness of sapphire enables a more accurate height measurement of the thickness of the lipid/fatty acid layers deposited on its surface. Figure 2e shows an example of the multi-lamellar structure of three monolayers of dipalmitoylphosphatidylcholine (DPPC) deposited by the Langmuir–Blodgett technique on a sapphire/Ag SERS substrate. The holes in the lipid structure reveal different thicknesses for each one of the consecutively deposited layers, where a monolayer has a typical measured height of 5 nm.

The SERS activity of the substrates was investigated with monolayers of R6G and p-ATP. Exposing R6G to visible wavelengths excites its fluorescence, which is broad and intense and totally covers its weaker Raman scattering. However, fluorescence is quenched in SERS. Therefore, obtaining the Raman spectrum of R6G on the substrates is a good indicator of successful SERS. p-ATP contains a thiol group (–SH) known to have a high chemical affinity to metal, enabling the molecule to adsorb to SERS substrates and form a single monolayer.[26] For these reasons, both R6G and p-ATP are commonly used in SERS studies.[26–28]

The prepared substrates were initially imaged with AFM to locate a large ordered area of at least 15 μm^2 containing a monolayer of molecules, ideal for performing SERS mapping. Within this image a 1–2 μm^2 region was selected to record a chemical mapping, as shown in Figs. 3a and 3e. Mappings were constructed by automated scanning of the sample through the focus of the laser, with a spatial resolution of less than 1 μm. The sample was moved in a raster pattern with step sizes of 50–100 nm, acquiring a SERS spectrum at each position at a rate of 2 s per pixel. The area of a Raman band in each spectrum was calculated after subtraction of a local linear baseline and used to build a spectral mapping. This mapping was then related back to the original AFM image, enabling direct correlation between SERS nanostructures and Raman scattering to reveal the exact position, orientation, and uniformity of enhancement across the substrate.

Raman bands at 1363 cm^{-1} for R6G (aromatic C–C and C–N stretching) and 1143 cm^{-1} for p-ATP (C–H bending and NH_2 rocking) were used to create the mappings (Fig. 3). The SERS substrates themselves have no Raman scattering, and therefore no background has been removed from the spectra. For both molecules, the mappings of the 1002 nm substrates provide information about the distribution of SERS enhancement, since the structure of the substrates can clearly be seen from the mappings (Figs. 3d and 3h). When compared to the AFM images taken of the same areas, regions of higher intensity pixels correspond to the position and orientation of the silver nanostructures while weaker SERS scattering was detected in between these nanostructures. These results suggest that for this type of substrate the SERS effect arises from the metallic surfaces themselves rather than from the gaps between them, which is in agreement with reported theoretical studies of these substrates.[22,29,30] The electric field enhancement has been calculated by comparing the SERS signal of p-ATP with the unenhanced Raman scattering from a neat solution of the molecule on a bare glass coverslip, taking into consideration the number of molecules sampled in each case.[22] An enhancement factor of $\sim 10^5$ was obtained for the substrates. It is important to note that for the mappings of the 384 nm substrates, it is not possible to identify individual nanostructures (Figs. 3b and 3c and Figs. 3f and 3g). Instead, these substrates provide a consistent enhancement of the Raman signal across large areas. The spatial resolution of a Raman spectroscopy system has a lower intrinsic threshold set by the diffraction limit, which is about 500 nm for our setup. In most cases this is a negative aspect as it restricts the size of surface features that can be resolved. However, using SERS substrates with nanostructures smaller than this limit provides enhancement that appears to be distributed evenly across the substrate. Therefore, the 384 nm substrates could be suitable for investigating nonuniform samples such as SLBs, for which

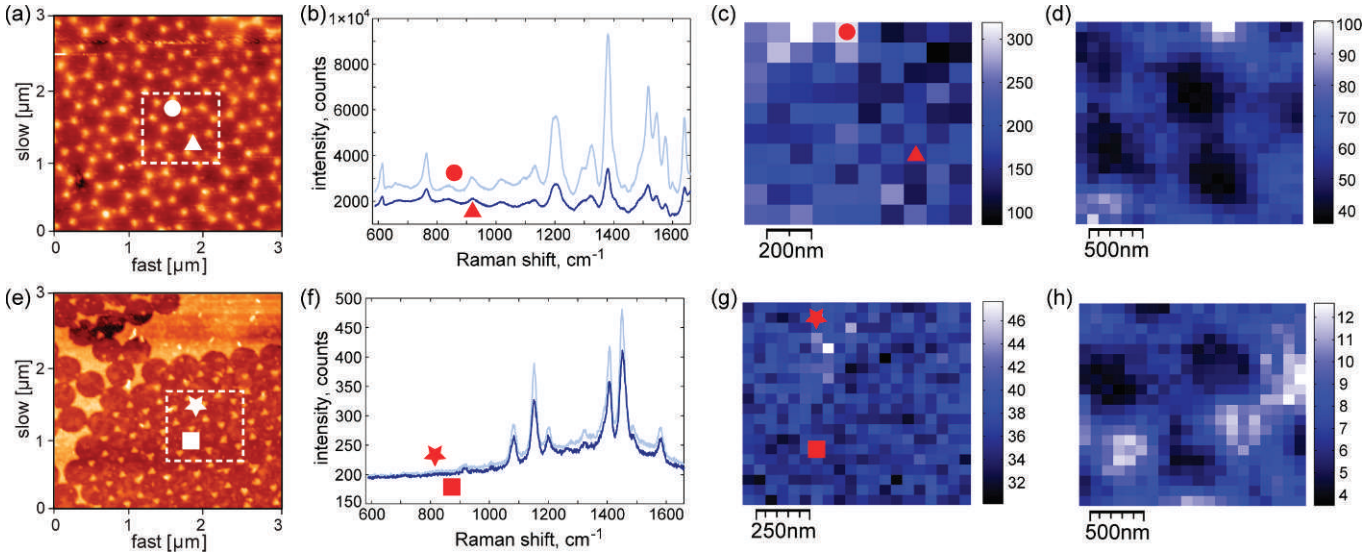

FIG. 3. AFM image of (**a**) R6G and (**e**) p-ATP on 384 nm substrates with (**b**, **f**) SERS spectra and (**c**, **g**) mappings recorded across the highlighted area (labeled spectra correspond to the scattering measured at the position of the same labeling in the images and mappings). (**d**, **h**) SERS mappings of the same molecules on 1002 nm substrates for comparison.

variation in SERS scattering across the sample can be used for spatially resolving the physiochemical properties of microdomains.

SERS of Fatty Acid and Phospholipid Bilayers. To demonstrate the capability of these SERS substrates to provide sufficient and uniform enhancement for imaging model cell membranes, layers of AA produced by LB were investigated on the substrates. AA is a fatty acid with a long alkyl chain of 20 carbons (C20:0). It is also a first approach towards more complex and nature-like or biomimetic systems, such as phospholipids, containing (among other components) two fatty acid chains. The integrated AFM–Raman system allows identification of the AA layers on the NSL substrates before measuring SERS spectra at selected locations (Fig. 4). The maximum thickness of the lipid distribution was found to be 10–15 nm, which suggests that each molecular layer of AA is about 3–5 nm in height, in agreement with previously reported results.[31,32] Raman spectra of AA powder was also included in Fig. 4d for peak comparison with the SERS signal obtained on the sapphire/Ag substrates.

The assignment of bands in the Raman spectra of lipids and fatty acids is well established;[33,34] however, those relating to the SERS spectra of these molecules are not as well known. Often the Raman and SERS spectra of a molecule vary,[35] due to the change in Raman spectroscopy selection rules that arise from the SERS effect.[36] SERS spectra often contain peaks that are slightly shifted in frequency from those in the Raman spectra or that are even absent. Alternatively, SERS spectra can contain additional Raman bands. In most cases, different bands exhibit different levels of enhancement. The main difference between the Raman spectra and the SERS of AA is the appearance of new bands in SERS at 1394 cm^{-1}. This band corresponds to symmetric CH_2 deformations and has been used previously to detect the presence of fatty acids from mixtures of fatty acids and lipids adsorbed on silver electrodes by SERS.[37] Vibrational modes at 1057, 1102, and 1122 cm^{-1} in the Raman spectrum of AA can be assigned to C–C trans stretching and relate to SERS peaks at 1059, 1102, and 1124 cm^{-1}. The Raman band at 1291 cm^{-1}, occurring at 1290 cm^{-1} in the SERS spectrum, denotes CH_2 twisting deformations. Peaks in the Raman spectrum at 1418, 1438, and 1464 cm^{-1} correspond to CH_2 scissoring and symmetric bending of the C–H bonds in the ester methyl group, and similarly the SERS vibration at 1394 cm^{-1}. An additional band is present in the

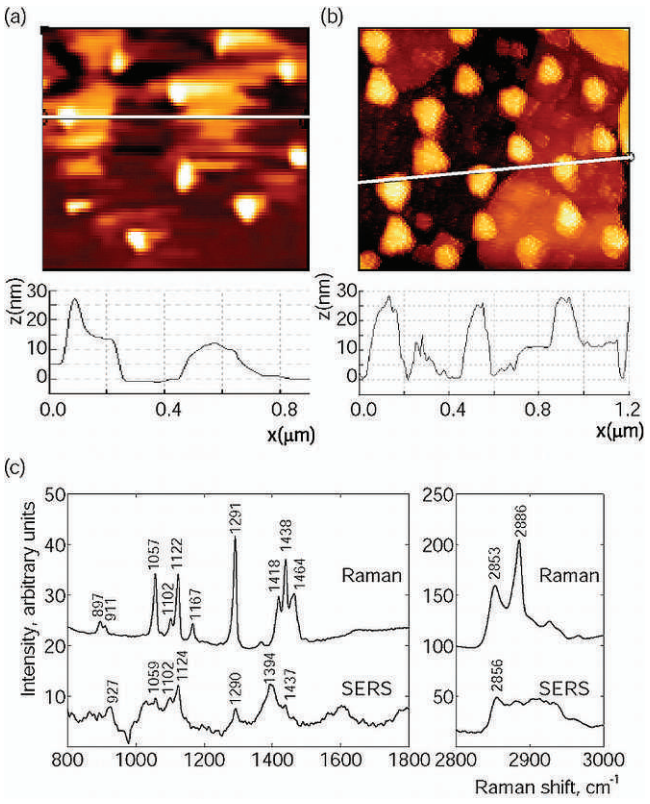

FIG. 4. Simultaneous AFM/SERS characterization of arachidic acid (AA) layers on a sapphire/Ag substrate: layers deposited (**a**) by the Langmuir–Blodgett method and (**b**) by spin coating. (**c**) Raman spectra of AA powder versus the SERS spectra of the multi-lamellar AA structure (laser power 56 μW at sample, 500 s, spectra were background corrected).

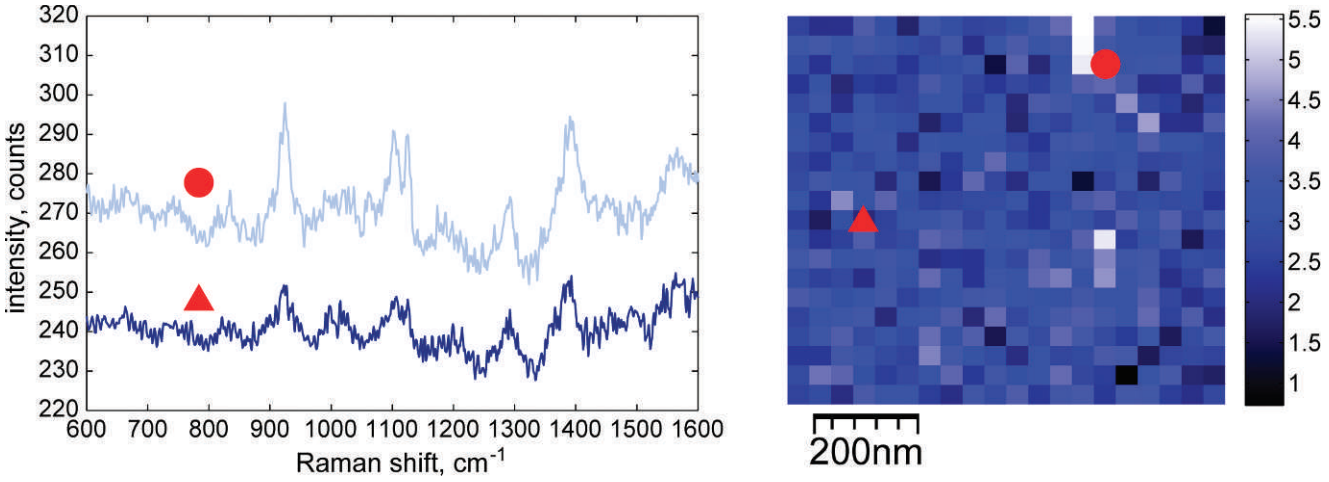

FIG. 5. SERS spectra and mapping of AA on 384 nm substrates (labeled spectra correspond to the scattering measured at the position of the same labeling in the mappings).

SERS spectrum of AA at 927 cm^{-1}; vibrational modes in the region of this peak can be assigned to acyl or C–C stretching, involving both the C–C and C–O bonds adjacent to the carbonyl group or the methyl terminal C–C bond.

To assess the suitability of the 384 nm SERS substrates for imaging AA layers and potentially investigating phase-separated microdomains, SERS mappings were measured as before using the Raman band at 1394 cm^{-1} (Fig. 5). The SERS chemical mappings highlight that scattering is detected over large areas of the substrate. The selected SERS spectra in Fig. 5 demonstrate that only small differences in enhancement can be detected between the "bright" and "dark" positions in the mapping, confirming uniform enhancement across the substrate. These results with a uniform homogeneous layer of AA show the potential of the NSL SERS-active substrates in imaging a single lipid bilayer both chemically and physically.

To expand the membrane model to more biologically relevant lipid chemical species, simultaneous AFM and SERS of DPPC layers were carried out (Fig. 6). Cationic DPPC was chosen to avoid the repulsion that globally neutral DPPC (but locally negatively charged due to acidic impurities) experienced on negatively charged substrates such as sapphire, thus improving the coverage of the SERS substrates. AFM images show a multi-lamellar structure where different thicknesses can be attributed to different numbers of layers, ranging from less than 5 nm (monolayer) to 15 nm (Fig. 6a). From the comparison with the Raman spectrum of powdered cationic DPPC in Fig. 6b, the SERS spectra show that the main Raman bands enhanced are the 1122 cm^{-1} band, corresponding to C–C stretching, the 1290 cm^{-1} band, related to C–H twisting deformations, and the spectral band at 1439 cm^{-1}, associated with C–H scissoring deformations. Also, a weak but reproducible band is observed at 1092 cm^{-1}, corresponding to C–C stretching.[38] The peak at 1057 cm^{-1}, also associated with C–C stretching, is very weak and can barely be detected over the background.

CONCLUSIONS

In this paper we have investigated NSL substrates in terms of their suitability for simultaneous topographical and SERS mapping of SLB by using an integrated AFM–Raman instrument. SERS substrates based on sapphire were chosen as they are flat within an error of 2 nm, showing their potential as planar platforms for lipid bilayer topographical imaging,

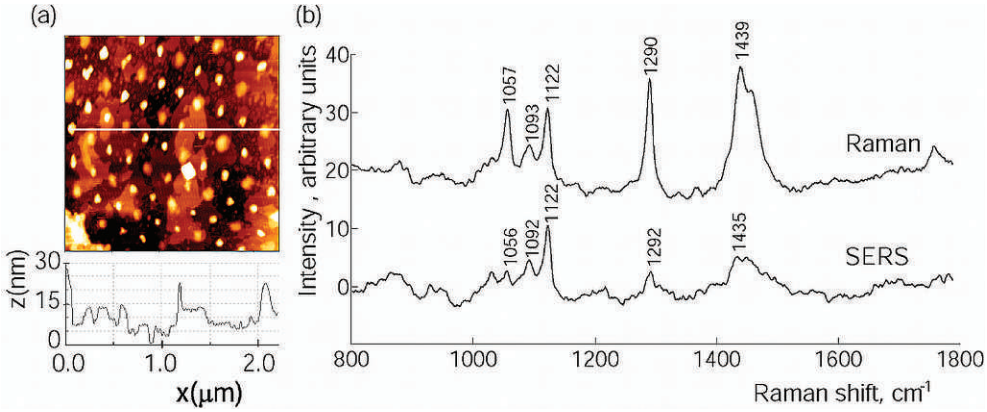

FIG. 6. Simultaneous AFM/SERS characterization of 3 monolayers of cationic DPPC on a sapphire/Ag substrate. (**a**) AFM image and line profile showing a thickness of the lipid multilayer structure of 5 nm (monolayer) to 15 nm (3 layers). (**b**) Raman spectra of bulk cationic DPPC powder and SERS spectra of the multi-lamellar lipid structure on sapphire/Ag substrates (laser power 56 μW at sample, 500 s, spectra were background corrected).

where phase-separated microdomains present height differences of the order of 2 nm.

High, uniform enhancement is important for detecting the weak scattering from these nanoscale structures and the variation in chemical composition of a lipid bilayer containing microdomains. SERS spectra and mappings of R6G and p-ATP monolayers have revealed the structure and variation in enhancement of the 1002 nm substrates, indicating that the highest signal occurs on the silver nanostructures themselves. Uniform enhancement was detected in similar mappings of the 384 nm substrates, for which the nanostructures are below the diffraction limit of the system. After topographical imaging by AFM, good signal-to-noise ratio SERS spectra of multi-lamellar structures of AA and cationic DPPC were obtained. Comparison between the Raman and SERS spectra enabled tentative assignment of the SERS bands. SERS mapping of AA layers was also performed to confirm the consistency and uniformity of the SERS enhancement. The AFM images of neutral DPPC monolayer stacking on sapphire/Ag SERS-active substrates show homogeneous layers of well-defined thickness distributed over the substrate. It was found that the SERS of DPPC was dominated by bands corresponding to the alkyl chains.

This study demonstrates the ability of combining AFM and SERS with NSL substrates for detecting SERS spectra of SLB. The flatness of the SERS substrates and the uniform enhancement of the Raman spectra show the potential of this technique for imaging phase-separated microdomains in heterogeneous planar SLBs. In addition, the AFM studies could be extended to include force spectroscopy, which could be used to relate the mechanical properties of the samples to the SERS spectral properties.

ACKNOWLEDGMENTS

We thank the UK Engineering and Physical Sciences Research Council (EPSRC) for financial support (EP/P502632/1). Also, thanks to Faris Sinjab (Nanoscience group, University of Nottingham) for the instrumental development of the accurate alignment of the laser with the AFM tip.

1. S. R. Shaikh, A. C. Dumaual, L. J. Jenski, and W. Stillwell, Biochim. Biophys. Acta **1512,** 317 (2001).
2. S. Munro, Cell **115,** 337 (2003).
3. K. El Kirat, S. Morandat, and Y. F. Dufrêne, Biochim. Biophys. Acta **1798,** 750 (2010).
4. C. M. Hebling, C. R. Morgan, D. W. Stafford, J. W. Jorgenson, K. D. Rand, and J. R. Engen, Anal. Chem. **82,** 5415 (2010).
5. A. Gunnarsson, F. Kollmer, S. Sohn, F. Hook, and P. Sjovall, Anal. Chem. **82,** 2426 (2010).
6. D. Lee, K. F. A. Walter, A.-K. Brockner, C. Hilty, S. Becker, and C. Griesinger, J. Am. Chem. Soc. **130,** 13822 (2008).
7. N. Kučerka, J. F. Nagle, J. N. Sachs, S. E. Feller, J. Pencer, A. Jackson, and J. Katsaras, Biophys. J. **95,** 2356 (2008).
8. V. Tiriveedhi and P. Butko, Biochemistry **46,** 3888 (2007).
9. M. Przybyło, A. Olżyńska, S. Han, A. Ożyhar, and M. Langner, Biophys. Chem. **129,** 120 (2007).
10. A. E. McKiernan, T. V. Ratto, and M. L. Longo, Biophys. J. **79,** 2605 (2000).
11. C. B. Fox, R. H. Uibel, and J. M. Harris, J. Phys. Chem. B **111,** 11428 (2007).
12. C. Lee and C. D. Bain, Biochim. Biophys. Acta **1711,** 59 (2005).
13. L. Li and J.-X. Cheng, J. Phys. Chem. B **112,** 1576 (2008).
14. E. O. Potma and X. S. Xie, Chem. Phys. Chem. **6,** 77 (2005).
15. G. W. H. Wurpel, J. M. Schins, and M. J. Müller, Phys. Chem. B **108,** 3400 (2004).
16. C. L. Leverette and R. A. Dluhy, Coll. Surf. A **243,** 157 (2004).
17. P. Krysinski, E. Zebrowska, B. Pałys, and Z. Łotowski, J. Electrochem. Soc. **149,** 189 (2002).
18. J. Kundu, C. S. Levin, and N. J. Halas, Nanoscale **1,** 114 (2009).
19. C. Heywang, M. Saint-Pierre Chazalet, M. Masson, and J. Bolard, Biophys. J. **75,** 2368 (1998).
20. J. Hrabakova, K. Ataka, J. Heberle, P. Hildebrandt, and D. H. Murgida, Phys. Chem. Chem. Phys. **8,** 759 (2006).
21. M. Saint-Pierre Chazalet, M. Masson, C. Bousquet, G. Bolbach, Y. Ridente, and J. Bolard, Thin Solid Films **244,** 852 (1994).
22. C. S. Sweetenham and I. Notingher, J. Nanophotonics **5,** 059504 (2011).
23. M. Larraona-Puy, A. Ghita, A. Zoladek, W. Perkins, S. Varma, I. Leach, H. Williams, A. A. Koloydenko, and I. Notingher, J. Biomed. Opt. **14**, 054031–1 (2009).
24. J. Rybczynski, U. Ebels, and M. Giersig, Coll. Surf. A **219,** 1 (2003).
25. L. Baia, M. Baia, J. Popp, and S. Astilean, J. Phys. Chem. B **110,** 23982 (2006).
26. C. Farcau and S. Astilean, J. Opt. A: Pure Appl. Opt. **9,** 345 (2007).
27. J. P. Schmidt, S. E. Cross, and S. K. Buratto, J. Chem. Phys. **121,** 10657 (2004).
28. J. Zhao, L. Jensen, J. Sung, S. Zou, G. C. Schatz, and R. P. Van Duyne, J. Am. Chem. Soc. **129,** 7647 (2007).
29. T.-H. Lin, N. C. Linn, L. Tarajano, B. Jiang, and P. J. Jiang, Phys. Chem. C **113,** 1367 (2009).
30. A. J. Haes, S. Zou, G. C. Schatz, and R. P. Van Duyne, J. Phys. Chem. B **108,** 6961 (2004).
31. D. P. E. Smith, A. Bryant, C. F. Quate, J. P. Rabe, C. Gerber, and J. D. Swalen, Proc. Natl. Acad. Sci. U.S.A. **84,** 969 (1987).
32. L. Bourdieu, P. Silberzan, and D. Chatenay, Phys. Rev. Lett. **67,** 2029 (1991).
33. R. E. Oakes, J. Renwick Beattie, B. W. Moss, and S. E. J. Bell, J. Mol. Struct. **626,** 27 (2003).
34. J. Renwick Beattie, S. E. J. Bell, and B. W. Moss, Lipids **39,** 407 (2004).
35. D. Maniu, V. Chis, M. Baia, F. Toderas, and S. Astilean, J. Optoelectron. Adv. Mater. **9,** 733 (2007).
36. M. Moskovits and J. S. Suh, J. Phys. Chem. **88,** 5526 (1984).
37. M. K. Weldon, V. R. Zhelyaskov, and M. D. Morris, Appl. Spectrosc. **52,** 265 (1998).
38. F. D. Gunstone, J. L. Harwood, and F. B. Padley, *The Lipid Handbook* (Chapman and Hall, New York, 1994).